DYNAMIC TENSILE RESISTANCE OF CONCRETE – SPLIT HOPKINSON BAR TEST

JOŠKO OŽBOLT[*], J. WEERHEIJM[†] AND AKANSHU SHARMA[††]

[*] Institute of Construction Materials, University of Stuttgart
Pfaffenwaldring 4, 70569 Stuttgart, Germany
e-mail: ozbolt@iwb.uni-stuttgart.de

[†] TNO Defence, Safety and Security, Rijswijk, The Netherlands
and Delft University of Thechnology
Computational Mechanics Group, Delft, the Netherlands
e-mail: j.weerheijm@tudelft.nl

[††] Reactor Safety Division
Bhabha Atomic Research Centre, Mumbai - 400085, India
e-mail: akanshusharma@yahoo.co.in

Key words: Concrete, Dynamic fracture, Rate sensitivity, Hopkinson bar, True and apparent strength, Finite elements, Microplane model

Abstract: The behavior of concrete structures is strongly influenced by the loading rate. Compared to quasi-static loading, on meso and macro-scale concrete loaded by impact loading acts in a different way. First, there is a strain-rate influence on strength, stiffness, ductility, and, second, there are inertia forces activated which influence the resistance and failure mode of concrete structure. The experimental and theoretical studies show that the influence of loading rate on tensile behavior of concrete is relatively strong. In dynamic testing the split Hopkinson bar (SHB) is used to measure concrete tensile resistance. The results of the experimental measurements show that after reaching some critical strain rate tensile resistance progressively increases with increase of strain rate. The questions discussed in the paper are: (i) what is the reason for progressive increase of tensile resistance ? and (ii) can the resistance be attributed only to material strength or are there some other effects ? To answer these questions the numerical analysis on a simple elastic-cohesive FE model is carried out. Moreover, simulation of the compressive pulse in a concrete bar, which is reflected from the free end-surface of the bar and causes tensile fracture, is carried out for different loading rates. The evaluation of the results clearly shows that the progressive increase of tensile resistance (apparent strength) can be attributed to structural inertia of the fracture zone, which is invoked by cracking of concrete and is not to the true material strength. It is shown that the size of the fracture process zone significantly influence apparent strength. Similar as the true strength it is also discussed that with the increase of strain rate concrete fracture energy does not increase progressively.

1 INTRODUCTION

The experimental and theoretical evidence show that loading rate significantly influences the resistance and failure mode of concrete structures [1-5]. In case of linear elastic material there is no rate sensitivity. However, in materials that exhibit damage and fracture phenomena, such as concrete, there is significant influence of loading rate on material and structural response. This implies

that rate sensitivity is closely related to damage (softening) of the material, i.e. more damage and higher level of heterogeneity (larger softening zone) will enhance the influence of loading rate on the structural response. Support for this statement can be found in the fact that concrete like materials exhibit the highest rate sensitivity.

Assuming that concrete is considered in the framework of meso or macro-continuum, the response of concrete structures depends on time dependent loading through three different effects [3,4]: (1) through the rate dependency of the growing micro-cracks (influence of inertia at the micro-crack level), (2) through the viscous behavior of the bulk material between the cracks (viscosity due to the water content) and (3) through the influence of structural inertia forces, which can significantly change the state of stresses and strains of the material. The first two effects can be accounted for by the constitutive law and the third effect should be automatically accounted for with dynamic analysis where the rate dependent constitutive law interacts with structural inertia at the material level [4]. Depending on the material type and the loading rate, the quasi-brittle materials, such as concrete, the first two effects are important for relatively low and medium strain rates. However, for higher strain rates (impact) the last effect dominates. Moreover, structural inertia cause the change of the failure mode, e.g. from mode one type of failure at low loading rates to mixed or punching type of failure at very high loading rates. Finally, inertia at the crack tip (fracture process zone) of a single propagating crack is also responsible for crack branching phenomena. As discussed by Ožbolt et al. [4], inertia changes the stress distribution around the crack tip, which force single crack to split into two cracks.

The experimental evidence shows that concrete under tensile load exhibits the strongest rate dependency. Sound experiments to study uni-axial tensile behavior of concrete is difficult even under static load. For dynamic testing split Hopkinson bar tests and spalling tests are used [6-11]. The results of experiments show that for strain rates larger than approximately $1\ s^{-1}$ the resistance increases progressively with the increase of strain rate. The question that arises and that is still under discussion is, what is the reason for such an increase and whether the experimentally measured resistance be attributed only to the material strength or also to other effects. This is discussed in the present contribution on hand of evaluation of theoretical and experimental results obtained from the split Hopkinson bar test.

2 RATE DEPENDENT STRENGTH – SPLIT HOPKINSON BAR

Hopkinson [12] experimentally tested behavior of various materials at high strain rates. On a long bar he generated compressive pulse by explosive charge or impacting bullet. On the end of the bar the compressive loading wave reflected as a tensile loading wave and cause fracture of brittle materials such as concrete, rock etc. Later, Kolsky [13] made the method operable for the practical measurements. The method, known as split Hopkinson (pressure) bar, is schematically shown in Fig. 1 for compressive testing.

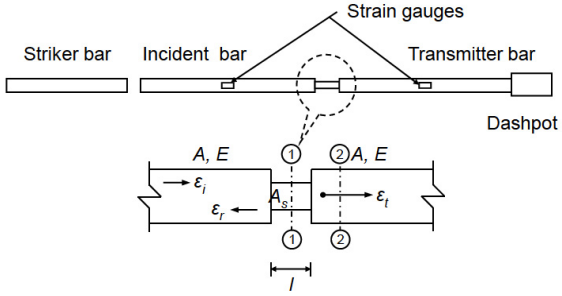

Figure 1: Schematic of split Hopkinson bar

The theory of uni-axial wave propagation through elastic media [13] leads to the following relations:

$$\varepsilon_s = -\frac{2c_0}{l}\int_0^t \varepsilon_r dt \quad \dot{\varepsilon}_s = -\frac{2c_0\varepsilon_r}{l} \qquad (1)$$

where c_0 is the wave propagation velocity, ε_r the reflected pulse in the incident bar and l the specimen length. The stress in the specimen can be calculated as:

$$\sigma_s = E\varepsilon_t \frac{A}{A_s} \qquad (2)$$

where E, A and ε_t are Young's modulus, cross-sectional area and transmitted pulse in the transmitter bar and A_s is the cross-sectional area of the specimen. High strain rates are reached if ε_r is large, which can be achieved by using a specimen diameter that is small compared to incident bar or in case when the bar material is much stiffer than the specimen. The incident, reflected and transmitted strain can be measured and then using Eq. (2) the stress in the specimen can be calculated as a function of strain rate from Eq. (1). By recording stresses σ_s at different strains ε_s it is also possible to calculate the fracture energy of concrete. In the analysis, no wave propagation within the specimen is taken into account and "static" equilibrium is considered. To neglect wave propagation, about three to five reverberations are needed to get equilibrium and uniform strain distribution. So the maximum strain rate in the SHB set-up also depends on the specimen length. A limitation that is not always taken into account in SHB tests.

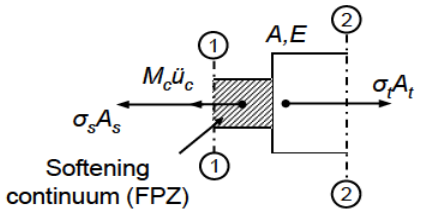

Figure 2: State of equilibrium of forces when concrete softens

For the interpretation of the experimentally observed rate effects in concrete, the question is whether the stress σ_s can be attributed only to the resistance of the material or there are some other effects that contribute to the stress σ_s. Fig. 2 shows the specimen between incidental and transmitted bar and the state of equilibrium of forces when concrete starts to get soften (softening continuum). From the equilibrium condition follows:

$$\sigma_s A_s + M_c\ddot{u}_c = \sigma_t A; \sigma_t = \frac{\sigma_s A_s + M_c\ddot{u}}{A_t}$$

$$\sigma_{t,s} = \frac{\sigma_s A_s}{A_t}; \quad \sigma_{t,I} = \frac{M_c\ddot{u}_c}{A_t} \qquad (3)$$

where M_c and $\ddot{u}_c$ are equivalent mass and acceleration of the concrete softening (cohesive) zone, respectively. Note that $\ddot{u}_c$ is the acceleration that is activated in the as a consequence of material softening. Obviously, under the condition that the material exhibit softening in non negligible part of the material volume (coarse quasi-brittle materials) the measured stress σ_t in the split Hopkinson bar test cannot be attributed only to material strength. It consists of the material resistance $\sigma_{t,s}$ and the contribution of inertia forces $\sigma_{t,I}$.

As mentioned before, in the framework of meso or macro-continuum the rate sensitive material resistance comes from the pre-peak rate dependent response (viscosity and rate dependent growth of micro-cracks) whereas the contribution of structural inertia comes from inertia forces that are activated as a consequence of softening that takes place in the fracture process zone. The larger the fracture process zone of the material is, the larger will be the contribution of inertia. Moreover, it can be expected that for the same width of the fracture process zone the influence of inertia will be stronger in case of larger specimen since then for the same crack extension the energy released from the structure is also larger. This will invoke higher accelerations in the process zone and consequently higher inertia forces will be activated. The above effects also confirm experimental observations, e.g. extremely brittle materials, such as glass, exhibit almost no rate sensitivity due to the fact that the size of the fracture process zone is very small [14].

From these considerations it is obvious that inertia effects in the material have to be incorporated in the analysis because they contribute to the apparent strength (see section 3) and do not present per definition the true material strength. For concrete the true strength is approximately a linear function of strain rate (log-log scale) and it is due to the

rate dependent microcrack growth and viscous behavior of cement paste of concrete [3,4,15]. This contribution can be accounted for by the constitutive law, which can be calibrated based on the experimental results for relatively low or medium strain rates, where inertia due to the softening is negligible. Although there are constitutive laws that explicitly account for the influence of structural inertia forces, the contribution of structural inertia forces ($\sigma_{t,I}$.) should come automatically from dynamic analysis, however, the constitutive law must be realistic in order to correctly account for the interaction with inertia [4]. It is important to note that as long as the modeling scale allows representing cracks individually no additional inertia term coupled to the softening volume need to be added to the constitutive law.

3 TRUE AND APPARENT DYNAMIC TENSILE RESISTANCE OF CONCRETE

To confirm theoretical considerations discussed in the previous section, finite element analyses for two geometries are carried out. In the first study a relatively simple cohesive-elastic FE model is investigated. The model principally corresponds to the measurement set-up of the split Hopkinson bar. Subsequently, the simulation of the compressive pulse in a concrete bar, which is reflected from the free end-surface of the bar and causes tensile fracture, is carried out. In numerical analyses as a constitutive law the rate dependent microplane model is used [4]. As regularization method a simple energy criterion (crack band method) is employed [16]. The numerical results are compared with experimental observations.

4 SIMPLE COHESIVE-ELASTIC FE MODEL

The geometry of the numerical specimen consists of two 3D eight-node solid finite elements. It is principally similar to the experimental set-up from Fig. 1. The first element is cohesive and represents a concrete specimen which after reaching tensile strength undergoes softening (micro-cracked continuum). The second element is linear elastic and corresponds to the part of the experimental set-up from Fig. 1. The properties of cohesive element (concrete) are taken as: Young's modulus $E_c = 30000$ MPa, Poisson's ratio $\nu = 0.18$, tensile strength $f_t = 3.5$ MPa, uniaxial compressive strength $f_c = 40$ MPa, concrete fracture energy $G_f = 0.09$ N/mm and mass density $\rho_c = 2400$ kg/m^3. It is assumed that the elastic element has the same elastic properties and density as the cohesive element. The model is loaded by controlling displacement rate of the nodes at the free surface of the elastic element in axial direction (see Fig. 3). Monitored are loading force and reaction. Compared to the experimental set-up from Fig. 1, the reaction represents true material resistance and the load is the resistance measured in the split Hopkinson bar test set-up. The analysis is performed for three different specimen sizes, $a = 25$, 50 and 100 mm, where a is element size. Note that in this simple model the size (volume) of the cohesive zone is equal to the element size.

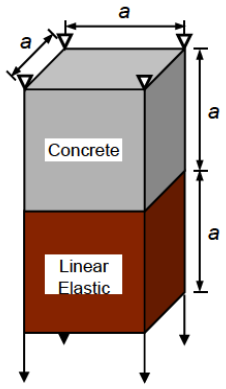

Figure 3: Simple cohesive-elastic FE model

For constant strain rate in static analysis the load and reaction must be the same. This is also the case in dynamic analysis but only if both elements are linear elastic. However, the question is whether they are the same in case of dynamic analysis, where the concrete element after reaching tensile strength undergoes softening. If they are not equal, the material resistance measured in the split Hopkinson bar test is not true material strength, i.e. it is the apparent strength.

In Fig. 4 are plotted typical reaction forces - and load-time response ($a = 50$ mm) for two different loading rates, 0.2 s^{-1} and 200 s^{-1}. The strain rates are calculated as prescribed displacement rate over the length of the cohesive element. For relatively low strain rate the load and reaction are almost the same, however, for very high strain rate the reaction is much smaller than the load. This implies that because of softening of the cohesive material the inertia forces are activated. They generate stresses in the elastic element that are much higher than the stresses in the cohesive element. Therefore, numerical results show that in general case the strength measured in the elastic element cannot be true material strength at high loading rates. This is apparent strength, which consists of the true material strength and the contribution of inertia forces, as discussed in previous section.

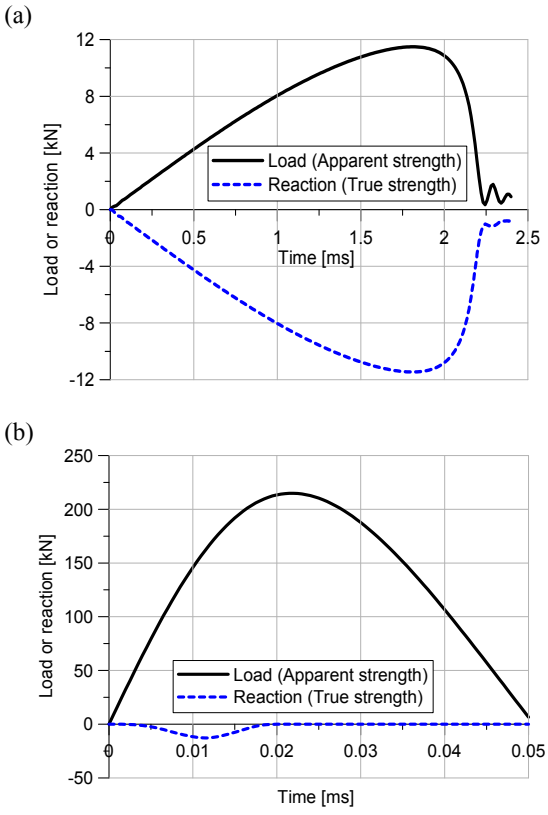

Figure 4: Typical reaction- and load-time response (a = 50 mm): (a) Strain rate = 0.2s^{-1} and (b) Strain rate = 200s^{-1}

Due to the fact that inertia forces are related to the size of the softening zone (FPZ), it can be expected that for brittle materials (e.g. glass) the influence of inertia on the apparent strength is negligible. To prove this the above analysis is repeated but assuming brittle behavior of cohesive element. The fracture energy of cohesive material is strongly reduced and taken as $G_f = 0.0009$ N/mm. All other properties are taken the same as before. In Fig. 5 are plotted reaction- and load-time response ($a = 50$ mm) for loading rate of 200 s^{-1} for brittle element. It can be seen that, in contrary to the cohesive element, for brittle element even at very high strain rates the reaction and load is nearly the same. This proves that for brittle material the strength measured in the elastic element is the same as true material strength, i.e. the apparent strength is nearly the same as true strength.

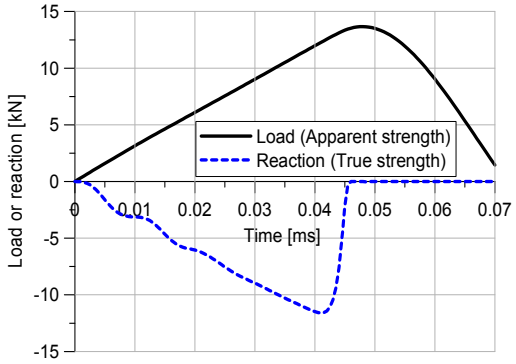

Figure 5: Typical reaction- and load-time response (a = 50 mm) of brittle material for strain rate of 200s^{-1}

Similar to the brittleness of the material, the size of the fracture process zone should have influence on inertia forces. Larger fracture zone should cause stronger influence of inertia on apparent strength. This also emerges from experiments, e.g. the Dynamic Increase Factor (DIF) of low quality concrete is larger than that of high quality concrete [17]. In Fig. 6a are plotted calculated DIF for true (reaction) and apparent (load) strength for three different specimen sizes ($a = 25$, 50, 100 mm) and for different strain rates. It can be seen that for the strain rates up to approximately 2 s^{-1} the true and apparent strengths are almost the same. However, for higher strain rates the true strength increases approximately linear in

semi-log scale whereas the apparent strength exhibits a progressive increase. As expected, the increase is stronger if the element size (size of the FPZ) is larger. In the contrary to this the true strength shows almost no sensitivity on the size of the element. Note that the increase of the true strength with increase of the strain rate is controlled by the energy activation theory which is the part employed microplane constitutive law.

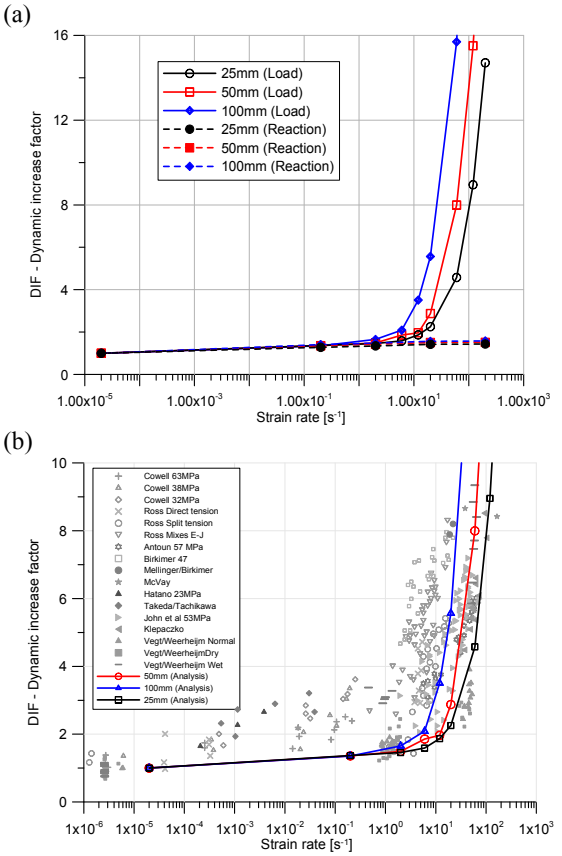

Figure 6: (a) Numerical results - apparent and true strength and (b) Comparison of numerically and experimentally observed apparent strength

In Fig. 6b are numerical results for apparent strength compared with the apparent strength measured in the experiments. The experimental data represents measurements on specimens of different sizes and shapes, different test methods, different concrete qualities and different content of water. Therefore, it is not surprising that there is relatively large scatter of test data with respect to the measured strain rate. It is surprising that in spite of very simple numerical model, the numerical results nicely fit a band of experimental results.

5 COMPRESSIVE PULSE IN A CONCRETE BAR

5.1 Numerical study

In the previous simple numerical example it is discussed that in the split Hopkinson bar test the experimentally measured rate dependent strength is not true strength but apparent strength, which is for very high strain rates much larger than the true material strength. In the second example the compressive pulse in a concrete bar (original Hopkinson bar), which is reflected from the free end-surface of the bar and causes tensile fracture, is carried out for different loading rates. The aim is to demonstrate the effect of high strain rates on material strength and concrete fracture energy by evaluating the results of the numerical analysis. Moreover, it will be demonstrated that because of inertia more than only one mode-I cracks in concrete specimen are generated.

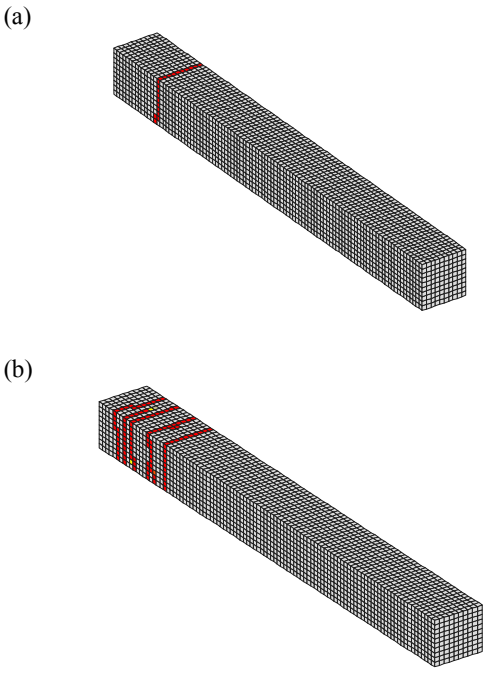

Figure 7: Typical failure modes for the bar at different lading rates: (a) 10 m/sec and (b) 40 m/sec.

The geometry, finite element discretization and loading of the concrete (1000x100x100 mm) can be seen on Fig. 7. To prevent local crushing of the concrete at the application of loading impulse, the bar is assumed to be confined in lateral direction (plane strain loading). The properties of concrete are taken as: Young's modulus $E_c = 30000$ MPa, Poisson's ratio $\nu = 0.18$, tensile strength $f_t = 2.75$ MPa, uniaxial compressive strength $f_c = 40$ MPa, concrete fracture energy $G_f = 0.06$ N/mm and weight density $\rho_c = 2400$ kg/m^3. Dynamic analysis is performed for different displacement rates that are applied at one end of the concrete bar. The applied displacements are: 0.5 mm/10^{-4}sec (loading rate 5 m/s), 1 mm/10^{-4}sec (loading rate 10 m/s), 2 mm/10^{-4}sec (loading rate 20 m/s) and 4 mm/10^{-4}sec (loading rate 40 m/s).

Figure 8a shows the DIF for true concrete strength as a function of strain rate. The strength is evaluated as an average strength over the single crack that is the closest to the free end of the bar. It can be seen that there is approximately a linear increase of strength with increase of strain rates in semi-log scale and that the fit of calculated data coincide with the data coming out of the constitutive law. For strain rates of 10, 65, 90 and 200 s^{-1}, DIF are 1.52, 1.51, 1.54 and 1.54, respectively. This was expected since the true material strength depends only on the constitutive law, i.e. on the outcome of the rate sensitive microplane model.

Fig. 8b plots the DIF for concrete specific and total fracture energy. The specific fracture energy is evaluated as the average fracture energy over the single crack that is the closest to the free end of the bar. Similar to the results obtained for dynamic strength, it can be seen that specific dynamic fracture energy of concrete exhibit approximately linear increase in semi-log scale. For the evaluated strain rates the corresponding values for DIF are 1.49, 1.56, 1.60 and 1.60, respectively. The increase of fracture energy is almost the same as the increase of strength. Since brittleness of the material is inverse proportional to fracture energy and proportional to the square of strength, as far as only one crack is considered it is obvious that with increase of strain rate brittleness increases. However, the increase of brittleness at high strain rate can be compensated by the fact that for high strain rates more than only one crack is generated. For strain rates of 65 and 200 s^{-1} the brittleness is almost the same. However, comparing Fig. 7a and 7b, it can be seen that in case of higher strain rate (Fig. 7b) the total energy consumed by fracture is much higher due to the multiple cracking and crack branching phenomena.

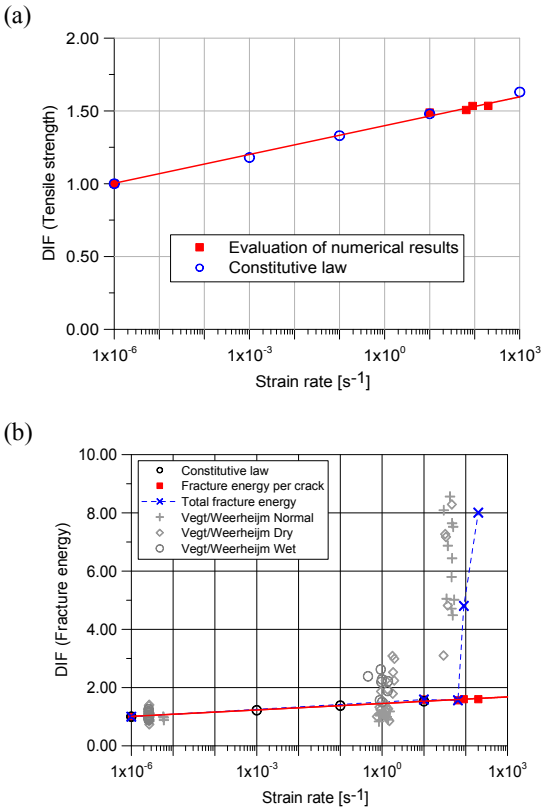

Figure 8: DIF for tensile strength (a) and for fracture energy as a function of strain rate (b)

If one accounts for the total fracture energy consumed by concrete specimen, instead only for the specific fracture energy (full line shown in Fig. 8b), then an increase of strain rate from 65 s^{-1} (single crack, see Fig. 7a) to 200 s^{-1} (approximately five cracks, see Fig. 7b) indicates progressive increase of the total fracture energy as a function of strain rate, as indicated by dotted line in Fig. 8b. Note that total fracture energy is simply estimated as the

specific fracture energy multiplied by the number of cracks, which increase with the increase of loading rate. From Fig. 8b can be seen that total fracture energy for higher strain rates agree well with measured data. But this data is for a single fracture zone. So either not all aspects are covered yet in the numerical simulations or, most probably, the data overestimate the fracture energy dramatically for a single fracture zone due to the contribution of inertia.

The evaluation of the numerical results shows that the true material strength is controlled by the rate dependent constitutive law, i.e. by the micro-cracking phenomena (inertia at the micro-cracking level) and viscosity at the pre-peak regime. The same is the case for fracture energy. The phenomena that control rate dependent strength and fracture energy are taking place at micro level. They should be distinguish from the effects of inertia forces at macro scale which are, among for some other effects, responsible for the apparent strength. In the here used rate sensitive microplane model the pre- and post-peak regime at the micro scale is modeled based on the energy activation theory. Due to the fact that the microplane model, similar to the discrete models, accounts for the interaction between different directions in the material the influence of structural inertia comes automatically from dynamic analysis.

6. EXPERIMENTAL EVIDENCE

From the previous sections it emerges that designing, performing and analysing dynamic (tensile) tests has to be done with great care. Combined experimental and numerical research is definitely preferred. The analyses showed that for the effect of inertia of the fracture zone on the apparent strength, the size of the fracture zone is important as well as the shape of the softening curve. Furthermore, it is shown that multiple fracture zones occur at high loading rates. In this section results of SHB and spalling tests will be presented focussing on these aspects.

Figure 9: SHB test set-up and instrumented specimen

At Delft a gravity driven SHB (see Fig. 9) for the modereate loading rate regime and a spalling set-up for the high loading rates are available. [7,9]. Notched specimen are used to exclude multiple fracture zones and the diagnostics are tailored to study the fracture energy. For the latter the fracture patterns are analysed and quantified by means of microscopy. Information on the test methods and diagnostics are given in e.g. [18,19]. In this paper the focus is on the results, but first some comments on the SHB and diagnostics.

In the gravity driven SHB a loading pulse with a long, linear ascending branch is generated and the specimen is loaded up to complete failure before the pulse maximum is reached. The SHB conditions mentioned in section 2 still count, therefore the strain rates for this set-up are limited to about 1/s.

In order to get information on the fracture energy notched specimen are used and the deformation of this zone is recorded as a function of time. Synchronizing these recordings with the transmitted stress pulse in the upper bar enables the construction of the stress- deformation, the softening curve.

To study the concrete response at the higher rates the spalling set-up with notched specimen was designed. The incident pressure pulse is generated with small explosive charges. Amplitude and duration are tuned to prevent damage in the compression phase and the occurrence of multiple fracture zones outside the notched area. In this set-up the stress conditions in the (notched) failure zone is determined using linear elastic wave propagation theory, assuming that the concrete

outside the single fracture zone is undamaged. Loading and assumption are determined and checked by means of multiple strain gauges (see Fig.10). The deformation of the fracture zone is recorded directly using a "massless" gauge. The stress-deformation curve emerges from the combined recordings.

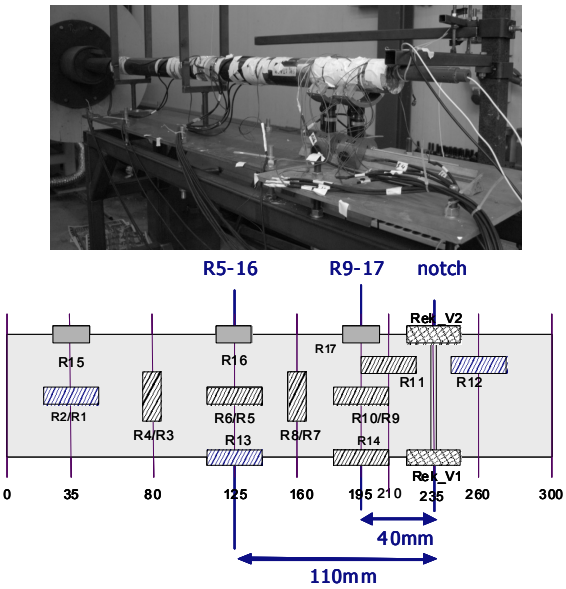

Figure 10: MSHB (modified SHB) set-up and instrumented specimen

In this set-up strain rates in the order of 200 1/s are reached. Note that the stresses transmitted through the fracture zone, the apparent strength, is recorded (gauge RG9-17, see Fig.11) which are affected by the inertia contribution of the fracture zone as discussed in the previous sections.

Static, SHB and spalling tests were performed for dry, normal and wet conditions. Details about composition, curing and test conditions are given in [18,19]. The characteristics for normal, lab curing conditions are: (i) cube compression strength 48 MPa, (ii) splitting tensile strength 3.4 MPa, (iii) Young's modulus 35 GPa and (iv) the max aggregate size 8 mm. In this paper only the data for the normal curing conditions are presented.

The experimental results on strength and fracture energy are summarized in Table 1. In the post-test microscopic analysis on "thin sections" the crack patterns were analyzed and quantified. Fig. 11 illustrates the kind of data that is obtained from the post test analysis. Some micro cracks are directly connected to the macro crack but most micro cracks are isolated in the fracture zone. The length of the macro cracks (l_{mac}), the length of connected micro cracks ($l_{mic,c}$) and isolated micro cracks ($l_{mic,i}$) were measured as well as the physical width (l_{FZ}) of the fracture zone. Especially the effect of the loading rate on the width of the softening zone is of interest for the discussion on the contribution of structural inertia to the apparent strength and fracture energy. The data is given in Table 2 for three loading rates. The diagnostics of the experiments enables to derive the load-deformation curve and to reconstruct the failure process in time. Figure 12 gives the curves for three loading rates.

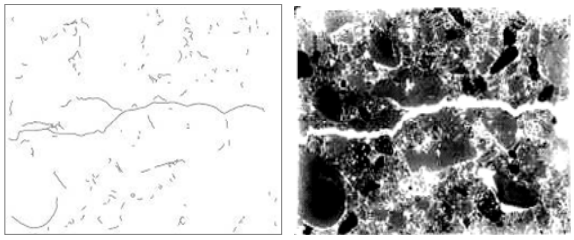

Figure 11: Post mortem crack pattern analysis

Table 1: Strength and fracture energy data

$\dot{\sigma}$ [GPa/s]	f_t [MPa]	G_f [N/m]	$\dot{\sigma}$ [GPa/s]	DIF_{Gf}
10^{-4}	3.30	120.2	1.0	1.0
40	5.58	120.4	1.7	1.0
1700	10.33	728.4	3.1	6.1

Table 2: Data on fracture patterns

$\dot{\sigma}$ [GPa/s]	l_{FZ} [mm]	l_{mac} [mm]	$l_{mic,tot}$ [mm]	DIF l_{micro}
10^{-4}	6.1	85	135	1.0
40	8.1	85	95	0.7
1700	19.1	85	162	1.2

Main observations for static and moderate load regime are (SHB): (i) The softening curves have two branches; (ii) The loading rate has no effect on: 2nd branch (macro crack), the length of the final macro crack, opening width of macro crack (i.e. δ_{frac}≈150 -200 μm)

and the width of the fracture zone; (iii) Up to $d\sigma/dt$= 40 GPa/s, no additional micro cracking occurs, it is even slightly reduced.

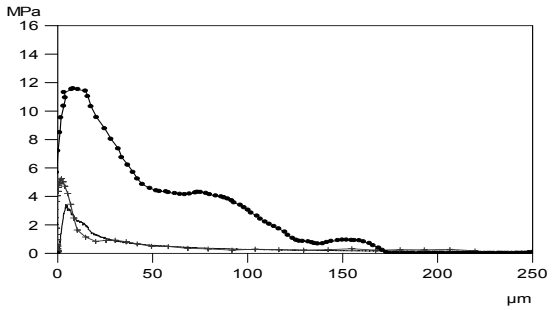

Figure 12: Stress-displacement curves for static, SHB and MSHB (modified SHB) tests

Referring to numerical modelling and the discussion on the contribution of inertia to the apparent material response at the higher loading rates, the observations on the load-deformation curves and the fracture energy need additional analysis.

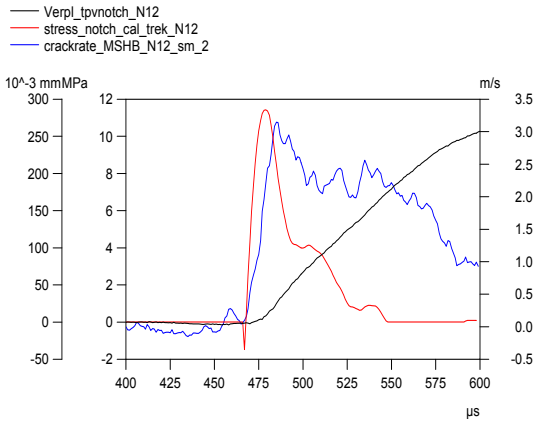

Figure 13: Stress $\sigma(t)$ - red curve, deformation $\delta(t)$- black curve and velocity $\delta(t)/dt$ - blue curve, recordings of the failure zone for spalling test

In the spalling tests on notched specimen the deformation of the single fracture zone was measured. From these recordings the velocity and also the acceleration of the material in the softening zone can be estimated. An example is given in Fig. 13 and will be used for a 1st order analysis. The recorded stress overestimates the true materials stress after non-linearity starts (at t = 472μs). Inertia affects the apparent strength until the maximum is recorded (at t = 478μs). In the elapsed time (Δt = 6 μs) the maximum mass that can be involved in micro cracking is within a distance to the "crack" of $\Delta t.c_p$ (≈ 20mm). The acceleration in Δt is about 2.10^5 m/s^2. Because the recorded acceleration is concentrated around the crack the inertia contribution to the apparent strength is in the order of 5 MPa which is in the same order as the enhanced strength increase related to the SHB tests. So the recorded strength is definitely affected by the structural inertia of the softening zone and so the measured fracture energy is.

Next step is the analysis of the whole softening process and so the fracture energy G_f. The post peak softening process can be schematized into two branches. The data of the moderate loading rate regime shows that the 2nd branch, the macro cracking, is not affected by the loading rate, neither by material or structural response. For the high loading regime the observations are quite different: (i) The two branches are still present, but much less obvious; (ii) The macro crack is fully opened at larger deformation (δ_{frac} ≈230 μm). The first part is affected by the inertia of the fracture zone as was shown for the pre-peak non-linearity phase. Because the total length of macro cracking is similar to the values for the other loading rates, it seems that the 2nd branch is also affected by structural inertia effects. The inertia might delay the opening of the macro crack and will be recorded as additional resistance. The recordings in Fig.13 show that during the 2nd branch the velocity, $\delta_{frac}(t)/dt$ is about constant. Which means that the additional resistance observed during the formation of the final macro-crack is not caused by structural inertia effects. However, there is another structural effect on the reconstructed stress-deformation curve in the spalling test. In the set-up, the reflected tensile wave interferes with the failure zone during the fracture process which results in additional stress pulse that propagates from the failure zone to the free end. This pulse travels forward and backward between the failure zone and the free end causing the "bumps" in the stress-deformation curves. Because of this phenomena and the recording of the apparent

strength the G_f values overestimate the true dynamic fracture energy.

Comparing above discussed numerical results with the results obtained by the test set-ups used in Delft it seems that for the low and moderate strain rates the measured and computed DIF for tensile strength and fracture energy agree well. However, for higher strain rates experimentally measured DIF for strength agrees well with apparent strength from the computations. The results for the fracture energy at high strain rates indicate that the structural inertia of the softening zone as well as the additional micro cracking and widening of the fracture zone cause the observed rate effects. Various phenomena occur and interfere during the dynamic softening process. Obviously, coordinated numerical and experimental work is needed for further clarifications and quantifying the true material response.

7 CONCLUSIONS

Based on the numerical results obtained in the study of rate dependent failure of concrete under tensile loading, the following can be concluded. (1) Loading rate has significant influence on the resistance and failure mode of concrete loaded in tension; (2) It is shown that for quasi brittle materials, such as concrete, material strength measured in indirect tensile test (split Hopkinson bar) is not the true material strength. It is the apparent strength, which consists of: (i) true material strength and (ii) the contribution of structural inertia forces generated as a consequence of material softening; (3) Numerical results suggest that the results of the tensile split Hopkinson bar and spalling tests need better interpretation, i.e. due to the fact that in the concrete specimen there is softening, the results of measurement should be corrected for the influence of inertia invoked by the softening; (4) The true strength is approximately a linear function of strain rate in log scale. It is controlled by the rate dependent crack growth at the micro scale (micro cracking) and by the viscosity due to the pore water content. In the numerical analysis comes out from the constitutive law; (5) Up to the strain rate of approximately 10 s^{-1} the true strength is nearly the same as apparent strengths. However, for higher strain rates there is a progressive increase of apparent strength, which is mainly attributed to structural inertia of the softening zone; (6) Quasi-brittle materials, which have relative large FPZ (e.g. low quality concrete) exhibit higher apparent strength than materials with smaller FPZ (high strength concrete); (7) It is shown that for brittle material, with small size of the FPZ (e.g. glass), the apparent and true strength are nearly the same; (8) Whether, similar to tensile strength, the true concrete fracture energy increases also linearly in log scale with increase of strain rate is not certain yet. Besides the strength increase also the amount of micro cracking and width of a single fracture zone increase. These aspects are not covered in the linear log scale relation; (9) It is demonstrated that in case of indirect tensile load (compressive bar) the number of tensile cracks depend on the loading rate. For relatively low loading rate only one tensile crack is generated, however, with increase of loading rate number of tensile cracks increases and damage is distributed over the large volume of the material; (10) True material strength should be accounted by the rate dependent constitutive law and the influence of structural inertia should automatically come from dynamic structural analysis. It is important to note that as long as the modeling scale allows representing cracks individually no additional inertia term coupled to the softening volume need to be added to the constitutive law. Therefore, the apparent strength should not be a part of the constitutive law; (11) For medium and low strain rates experimental results agree with numerical prediction, however, for higher loading rates from measured strength and fracture energy data the influence of the inertia forces must be correctly filter out in order to correctly predict true rate dependent material properties. With this respect further numerical and experimental work is needed.

REFERENCES

[1] Bischoff, P. and Perry, S., 1991. Compressive behaviour of concrete at high strain rates. *Mat. and Str.*, **24**: 425-450.

[2] Reinhardt, H.W. and Weerheijm, J., 1991. Tensile fracture of concrete at high loading rates taking account of inertia and crack velocity effects. *Int. J. of Fract.*, 51: 31.

[3] Ožbolt, J., Rah, K. K. and Mestrović, D., 2006. Influence of loading rate on concrete cone failure. *Int. J. of Fract.*, **139**:239–252.

[4] Ožbolt, J., Sharma, A. and Reinhardt, H. W., 2011. Dynamic fracture of concrete – compact tension specimen. *Int. J. of Solid and Structures*, **48**: 1534-1543.

[5] Ožbolt J. and Sharma, A., 2012. Numerical simulation of dynamic fracture of concrete through uniaxialtension and L-specimen. *Eng. Fract. Mech.*, **85**: 88-102.

[6] Reinhardt, H. W., Körmeling, H. A. and Zielinski, A. J., 1985. The split Hopkinson bar, a versatile tool for the impact testing of concrete. *Mat. and Str.*, Vol. 19, **109**: 55-63.

[7] Weerheijm, J., 1992. *Concrete under impact tensile loading and lateral compression*. Dissertation, TU Delft, the Netherlands.

[8] Weerheijm, J. and van Doormaal J.C.A.M., 2004. *Tensile failure at high loading rates; Instrumented spalling tests*. International Conference FramCoS 5.

[9] Weerheijm, J., van Doormaal, J.C.A.M., 2007. Tensile failure of concrete at high loading rates: new test data on strength and fracture energy from instrumented spalling test. *Int. J. Impact Eng*. **34**: 609–626.

[10] Pedersen, R. R., 2009. *Computational Modelling of Dynamic Failure of Cementitious Materials*. Dissertation, TU Delft, the Netherlands.

[11] Schuler, H., 2004. *Experimentelle und numerische Untersuchungen zur Schädigung von stoßbeanspruchtem Beton*. Dissertation, Universität der Bundeswehr München, Gernany.

[12] Hopkinson, B., 1914. A method of measuring the pressure produced in the detonation of high explosives or by the impact of bullets. *Phil. Trans. Roy. Soc. London*, Series A, Vol. 213, **10**:437-456.

[13] Kolsky, H., 1953. *Stress waves in solids*, Clarendon Press, Oxford.

[14] Peroni, M., Solomos, G., Pizzinato, V. And Larcher, M., 2011. Experimental investigation of high strain-rate behaviour of glass. *Applied Mechanics and Materials*, **82**:63-68.

[15] Mihashi, H., Wittmann, F.H., 1980. Stochastic approach to study the influence of rate of loading on strength of concrete. *HERON*, 25(3).

[16] Bažant, Z. P. and Oh, B. H., 1983. Crack band theory for fracture of concrete. *RILEM*, **93**(16), 155-177.

[17] *fib*, 2010. *New Model Code*. Chapter 5, Code-type models for concrete behavior (Draft).

[18] Vegt, I. Breugel, K. van and Weerheijm, J. 2007. *Failure mechanisms of concrete under impact loading*. FraMCoS-6, Catania, Italy, 17-22.

[19] Vegt, I. Weerheijm, J. and Breugel, avn K., 2009. *The rate dependency of concrete under tensile impact loading Fracture energy and fracture characteristics*. Proceedings of 13th ISIEMS.